Photoacoustic tomography of small animal brain with a curved array transducer

Xinmai Yang
Washington University in St. Louis
Department of Biomedical Engineering
Optical Imaging Laboratory
St. Louis, Missouri 63130

Anastasios Maurudis
John Gamelin
Andres Aguirre
Quing Zhu
University of Connecticut
Department of Electrical Engineering
Storrs, Connecticut 06269

Lihong V. Wang
Washington University in St. Louis
Department of Biomedical Engineering
Optical Imaging Laboratory
St. Louis, Missouri 63130

Abstract. We present the application of a curved array photoacoustic tomographic imaging system that can provide rapid, high-resolution photoacoustic imaging of small animal brains. The system is optimized to produce a B-mode, 90-deg field-of-view image at sub-200-μm resolution at a frame rate of ~1 frame/second when a 10-Hz pulse repetition rate laser is employed. By rotating samples, a complete 360-deg scan can be achieved within 15 s. In previous work, two-dimensional (2-D) *ex vivo* mouse brain cortex imaging has been reported. We report three-dimensional (3-D) small animal brain imaging obtained with the curved array system. The results are presented as a series of 2-D cross-sectional images. Besides structural imaging, the blood oxygen saturation of the animal brain cortex is also measured *in vivo*. In addition, the system can measure the time-resolved relative changes in blood oxygen saturation level in the small animal brain cortex. Last, ultrasonic gel coupling, instead of the previously adopted water coupling, is conveniently used in near-real-time 2-D imaging. [DOI: 10.1117/1.3227035]

Keywords: photoacoustics; imaging; imaging systems.

Paper 08423R received Dec. 2, 2008; revised manuscript received Jun. 26, 2009; accepted for publication Jul. 14, 2009; published online Sep. 16, 2009.

1 Introduction

In recent years, photoacoustic imaging (PAI, also referred to as optoacoustic or thermoacoustic imaging) has emerged as a promising novel biomedical imaging modality.[1–5] As a hybrid imaging modality, PAI can provide ultrasound-resolution images with intrinsic optical contrast in regions up to 5 cm deep.[6,7] Besides structural information, PAI can also detect functional changes and disorders *in vivo*[8,9] since these changes and disorders usually induce local optical contrast through changing blood volume and oxygenation. Therefore, PAI represents a novel technology from the perspectives of both ultrasound and optical imaging: it adds new contrast and functional information to ultrasound imaging, and it greatly extends the depth of high-resolution optical imaging.

In the past decade, as small animal models have been established for many human diseases, *in vivo* small animal imaging techniques have developed dramatically. PAI has attracted much attention in this area due to the aforementioned merits. In particular, reconstruction-based PAI—photoacoustic tomography (PAT)—has been successfully applied to small animal brain imaging, and its applications in structural, functional, and molecular imaging have been demonstrated.[8–10]

Frequently, PAT involves the scanning of a single ultrasound detector. The use of a single detector is inexpensive and can provide a good signal-to-noise ratio (SNR) for an image; however, the data acquisition duration is long, usually ~20 min per cross section. The prolonged measurement time presents great challenges for the control of small animal physiological parameters, especially when time-resolved functional information is desired or multiple slices of cross-section images are needed. Therefore, real-time or near real-time PAT scans are necessary, which may be realized by using array transducers.

The use of ultrasound array transducers for PAT has been explored by several groups.[11–18] In these studies, linear or curved array transducers were employed to reduce data acquisition time and meet clinical needs. However, these systems are neither designed nor optimized for small animal use. We have developed a curved array photoacoustic system optimized for high-resolution tomography of small animal brains.[19] The array was custom fabricated by Imasonic, Inc. (Besançon, France), using piezocomposite technology for high sensitivity and SNR. The system employs 128-element ultrasonic transducers operating at 5 MHz with 80% bandwidth for resolution of fine features such as brain vasculatures, while retaining high sensitivity for deep imaging. To mimic the scanning of a single element transducer, all the elements are arranged to form a quarter circle of 25 mm radius; therefore, it takes three rotations to get the 360-deg view data. Each individual element has an elevation height of 10 mm with an azimuthal pitch of one wavelength (0.308 mm) and a kerf of 0.1 mm. Furthermore, each element is cylindrically focused with a focal distance of 19 mm.

Address all correspondence to: Lihong Wang, Washington University in St. Louis, Department of Biomedical Engineering, Optical Imaging Laboratory, St. Louis, MO 63130. Tel: (314) 935-6152; Fax: (314) 935-7448; E-mail: lhwang@biomed.wustl.edu

1083-3668/2009/14(5)/054007/5/$25.00 © 2009 SPIE

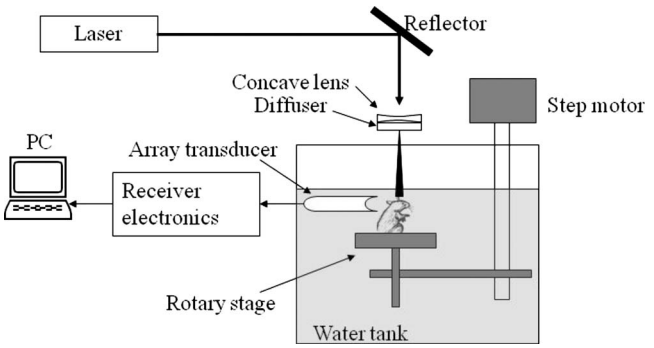

Fig. 1 Schematic of the curved array photoacoustic tomography system.

In the case of a 360-deg scan, this focusing effect results in a uniform central imaging region of approximate 16 mm in diameter. A 16-channel data-acquisition module and dedicated channel detection electronics allow capture of a 90-deg field-of-view image in less than one second when a 10-Hz pulse repetition rate laser is employed, and a complete 360-deg scan can be achieved through sample rotation within 15 s.

The technical design and systematic evaluation of this system has been reported in detail previously.[19,20] The main purpose of current paper is to demonstrate that this curved array is capable of *in vivo* small animal brain imaging, especially for functional imaging. Since the curved array was designed for small animal functional brain imaging, to test and demonstrate its capability is the first step for more complex brain functional detection in the future. We report the applications of the system on small animal brain imaging, including 3-D cross-sectional brain imaging, *in vivo* brain cortex imaging, and near real-time hemodynamic detection on a rat brain cortex. The results suggest that the current system can perform PAT of small animal brains to provide both structural and functional information *in vivo*.

2 Methods and Materials

The schematic for the noninvasive photoacoustic tomography of rat brains is shown in Fig. 1. A Q-switched Nd:YAG laser (LS-2137/2, LOTIS TII)–pumped tunable Ti:sapphire laser (LT-2211A, LOTIS TII) was employed to provide laser pulses with a FWHM <15 ns, a pulse repetition rate of 10 Hz, and a wavelength range of 750 to 820 nm. The incident energy density of the laser beam was controlled to be less than 15 mJ/cm^2 on the surface of the animal head, which is well below the ANSI limit.[21] The beam was diverged with a concave lens and homogenized by a circular diffuser to produce a uniform illumination of approximately 20 mm in diameter at the sample. The laser light was positioned at the center of curvature of the transducer and illuminated the sample orthogonal to the imaging plane of the transducer for maximum uniformity.

In the animal experiments, Sprague Dawley rats (60 100 g body weight) or Swiss Webster mice ($\sim$25 g body weight; from Harlan Sprague Dawley, Inc., Indianapolis) were used. For *in vivo* tests, a small animal was initially anesthetized by the intramuscular injection of a mixture of 87 mg/kg ketamine plus 13 mg/kg xylazine. Subsequent anesthesia was achieved by the inhalation of a mixture of O_2 and isoflurane. Before experiments, the hair on the head of the small animal was depilated using hair removal lotion. The mouth and nose of the animal were covered with a breathing mask to deliver oxygen and anesthesia gas. A custom-designed animal holder was used to fix the head of the animal with ear-pins and a tooth-pin. The animal was placed in sitting position, and the body of the animal was secured with surgical tapes to provide support to the animal. During experiments, the small animal and the animal holder were mounted on a rotary stage positioned at the center of the curved array transducer. The rotary stage could be turned in 90-deg increments to simulate the angular view of a full ring array. The head of the small animal was adjusted so that the brain cortex surface was parallel with the imaging plane. After the data acquisition for PAT, the animal was sacrificed by the intraperitoneal injection of highly concentrated pentobarbital.

In the measurements of blood oxygenation, we assumed that deoxyhemoglobin (Hb) and oxyhemoglobin (HbO_2) were the dominant absorbing compounds in blood at two wavelengths λ_1 and λ_2. Relative total hemoglobin concentration (rHbT) and blood oxygen saturation (SO_2) could then be calculated using the detected optical absorptions at the two applied wavelengths:[22–24]

$$\mathrm{rHbT} = [\mathrm{HbO_2}] + [\mathrm{Hb}] = \frac{\mu_a^{\lambda_1}\Delta\varepsilon_{Hb}^{\lambda_2} - \mu_a^{\lambda_2}\Delta\varepsilon_{Hb}^{\lambda_1}}{\varepsilon_{Hb}^{\lambda_1}\varepsilon_{HbO_2}^{\lambda_2} - \varepsilon_{Hb}^{\lambda_2}\varepsilon_{HbO_2}^{\lambda_1}}, \quad (1)$$

$$\mathrm{SO_2} = \frac{[\mathrm{HbO_2}]}{[\mathrm{HbO_2}] + [\mathrm{Hb}]} = \frac{\mu_a^{\lambda_2}\varepsilon_{Hb}^{\lambda_1} - \mu_a^{\lambda_1}\varepsilon_{Hb}^{\lambda_2}}{\mu_a^{\lambda_1}\Delta\varepsilon_{Hb}^{\lambda_2} - \mu_a^{\lambda_2}\Delta\varepsilon_{Hb}^{\lambda_1}}, \quad (2)$$

where μ_a is the absorption coefficient; ε_{Hb} and ε_{HbO_2} are the known molar extinction coefficients of Hb and HbO_2, respectively; $\Delta\varepsilon_{Hb}=\varepsilon_{HbO_2}-\varepsilon_{Hb}$; and [Hb] and [$HbO_2$] are the concentrations of the two forms of hemoglobin, respectively. By irradiating an animal head with light at two different wavelengths, λ_1 and λ_2, independently, we could get two photoacoustic images that represent the distributions of the optical energy deposition in the cerebral cortex corresponding to the two wavelengths. The optical energy deposition is dependent on the optical absorption and the light fluence at specific location. Considering that the skin and skull covering the brain are relatively homogeneous, the light fluence in the brain cerebral cortex is similarly homogeneously distributed in the horizontal plane at the two wavelengths. We can then calculate the images of an absolute estimation of SO_2 based on Eq. (2).

3 Results and Discussions

Three-dimensional (3-D) PAT brain images of a mouse were obtained *in situ* noninvasively as a series of 2-D cross sections. The animal was sacrificed before the experiment, mounted to the rotary stage, and then immersed in the water tank. The laser wavelength used was 797 nm. Figure 2 shows the PAT cross sections at different brain horizontal planes. Figure 2(a) shows the cortex surface. Figures 2(b)–2(e) show the interior brain structures underneath the superficial cortex with a 2-mm increment along the depth. To illustrate the features shown in these PAT images, we have labeled some char-

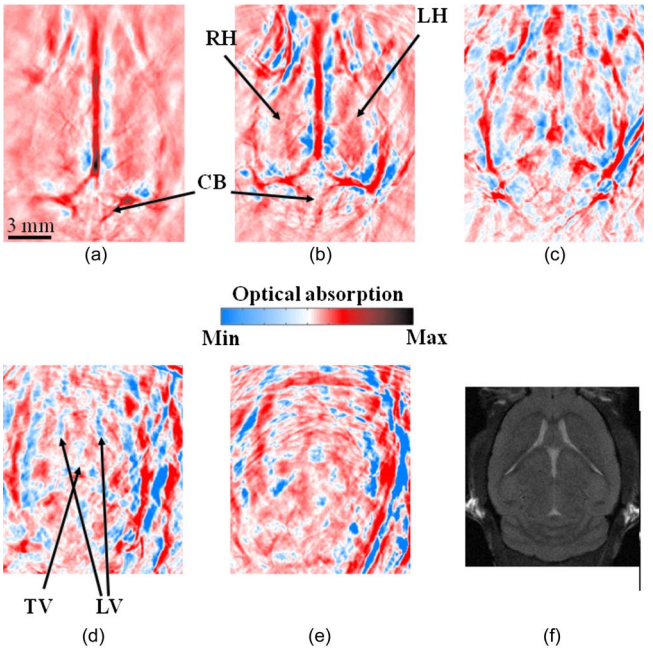

Fig. 2 *In situ* 3-D mouse brain images obtained by the curved array photoacoustic tomography system. The images show horizontal cross sections from the dorsal to the ventral part of the brain, where the imaging depth is (a) 0 mm, (b) 2.0 mm, (c) 4 mm, (d) 6 mm, and (e) 8.0 mm from the top surface of the mouse's brain, with an interval of 2 mm. Major tissue structures are indicated on the images. An MRI image at a similar depth as (d) is shown in (f). The color bar shows the relative magnitude of optical absorption. CB: cerebellum; RH: right hemisphere; LH: left hemisphere; LV: lateral ventricle; TV: third ventricle. (Color online only.)

acteristic tissue structures. An MRI image at a similar depth as Fig. 2(d) is presented in Fig. 2(f) and shows good similarities. In Fig. 2(d), the ventricular system is clearly visible on the image.

By rotating the sample, better quality images can be obtained; however, the data acquisition speed is reduced. To get near real-time imaging, we avoided rotation. With the current quarter-ring array, we can have a 90-deg view angle if no rotation is employed. Although the image quality is degraded and some information may be missing because of the incomplete data captured with no rotation, there are distinct advantages. First, near real-time PAT images can be acquired, which allow us to monitor the time-resolved change in a small animal. Second, instead of using water as the coupling material between the transducer array and a sample, ultrasound gel can be used as the coupling medium without worrying about coupling problems caused by rotation. In PAT experiments reported in the literature, water tanks have been used to hold water for coupling while the detection transducer was scanned. The use of ultrasound gel is much more convenient. Furthermore, although with a 90-deg view angle, the information about the image is incomplete, we can focus on the structures of interest one at a time without monitoring the whole image.

Figure 3 shows an *in vivo* rat cortical cortex image obtained with the curved array without rotating the transducer. This image was obtained by using ultrasound gel as coupling

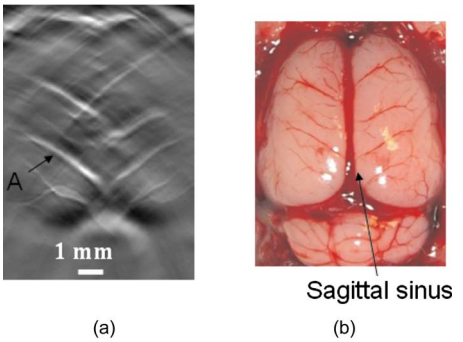

Fig. 3 PAT image from the curved array system without any rotation, i.e., only a 90-deg view angle. (a) PAT image; (b) open-skull photograph.

material; therefore, a water tank is not needed for this case. To get complete structural information, a 360-deg view angle is required.[25] Because only 90-deg view angle data was acquired in the current situation, some structures are missing from the image, including, notably, the sagittal sinus, which is labeled in the open-skull photograph. However, Fig. 3(a) still shows most of the blood vessels on the cortical surface, which are oriented perpendicular or nearly perpendicular to the sagittal sinus, and exhibits a good match with the open-skull photograph shown in Fig. 3(b). Most important, this PAT image was acquired within ~1 s, which is nearly real-time monitoring. Therefore, with the current curved array, we can provide fast-frame images at ~1 frame/second. The fast frame rate allows us to monitor the changes in these blood vessels in Fig. 3(a) as a function of time.

Figure 4 shows the *in vivo* measured photoacoustic signal strength as a function of time as the blood oxygenation level on the rat brain cortex changes. The signal strength was obtained from the single blood vessel indicated as A in Fig. 3(a). The animal experienced two physiological statuses: normoxia and hyperoxia. Figure 4(a) shows the hemodynamic changes on the rat brain cortex when the physiological status changed from normoxia to hyperoxia, and Figure 4(b) shows the hemodynamic result when it changed from hyperoxia to normoxia. The laser wavelength used was 771 nm. At this wavelength, deoxyhemoglobin has a greater extinction than

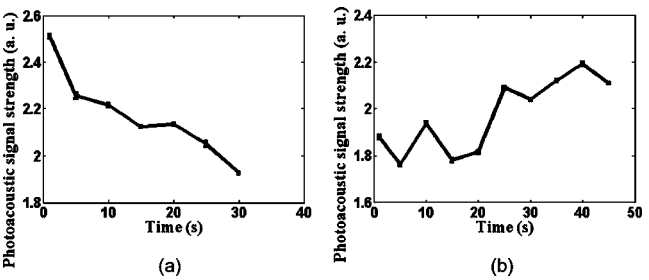

Fig. 4 Rat brain cortex hemodynamics with the curved array transducer. (a) The photoacoustic signal strength change on the rat brain cortex when the physiological status changed from normoxia to hyperoxia; (b) the photoacoustic signal strength change when the physiological status changed from hyperoxia to normoxia. The laser wavelength was 771 nm. The error bars are the standard errors at each measurement point.

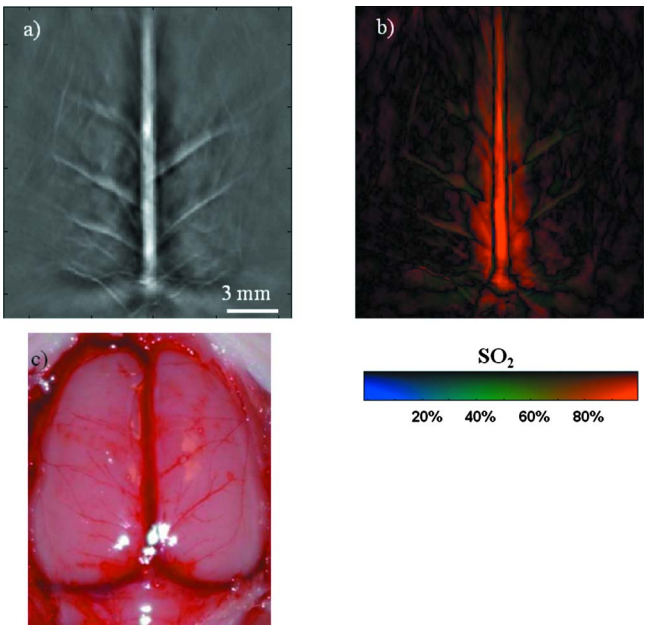

Fig. 5 *In vivo* measurement of a rat brain cortex with a 270-deg scan angle. (a) Structural image; (b) SO_2 distribution on the rat brain cortex; (c) open-skull photograph. The SO_2 values were calculated from the blood vessels shown on the cortex surface.

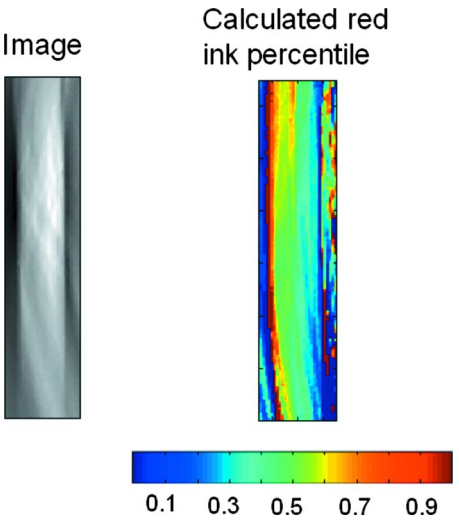

Fig. 6 Image of a plastic tube filled with the mixture of red/blue ink. The mixture ratio between red and blue ink is 50:50. (Color online only.)

oxyhemoglobin. Because the hyperoxic state carries less deoxyhemoglobin than the normoxic state, we observed a decrease in the strength of the photoacoustic signals in Fig. 4(a) and an increase in the strength of the photoacoustic signals in Fig. 4(b).

Figure 5 shows an *in vivo* measurement of a rat (~90 g body weight) brain cortex with a 270-deg scan angle, i.e., the animal was rotated twice to receive photoacoustic signals generated at the brain cortex from a 270-deg angle. Because rotations were required to obtain this image, we have to use water as the ultrasound coupling material, and the experiment was conducted in a water tank. Figure 5(a) shows the structural image, which matches very well with the open-skull photograph shown in Fig. 5(c). To obtain the SO_2 distribution on the rat brain cortex, we acquired images with laser wavelengths of 797 nm and 762 nm. At the isosbestic 797-nm wavelength, deoxy- and oxyhemoglobin have the same molar optical extinction coefficients. At 762 nm, the optical extinction coefficient of deoxyhemoglobin is about 2.5 times of that of oxyhemoglobin. At each scanning position, images were acquired in one minute for both wavelengths, and then the SO_2 values were calculated by Eq. (2). Figure 5(b) shows calculated SO_2 on the rat brain cortex. The results show reasonable SO_2 distributions in the blood vessels of the rat cerebral cortex (except in the sagittal sinus), with most large blood vessels on the cerebral cortex having low SO_2 values. This measurement is consistent with the fact that the vessels shown on the image close to the sagittal sinus are draining veins. However, the SO_2 value calculated in the sagittal sinus is inconsistent with the fact that the sagittal sinus contains venous blood. This inconsistency is due to the poor depth resolution (the resolution along the z direction). Along the depth at the location of the sagittal sinus, there are arteries and veins. Due to poor depth resolution, PAT picked up all the signals from that location, which in turn caused inaccurate SO_2 calculations.

To further understand the reliability of blood oxygenation measurement in Fig. 5, we have conducted an *in vitro* test. In the *in vitro* test, PA signals generated from a clear plastic tube filled with a mixture of red and blue India ink are measured. The ratio of the red and blue ink in the mixture was carefully controlled to be 50:50. After the measurement of the mixture, PA waves generated by red ink only in the clear plastic tube will be detected in water, and the amplitude is recorded as A_r. Then PA pulses with the same energy level at the same wavelength are used to induce PA waves from blue ink in the same clear plastic tubes, and the amplitude is recorded as A_b. Because A_r and A_b are obtained with the same setting, we further assume that the red and blue ink have similar thermal properties. Therefore, A_r and A_b can be used as relative optical absorption coefficients (related to the absolute optical absorption coefficient with the same constant) of red and blue India ink at this particular light wavelength. The measurements were made at 797-nm and 762-nm light wavelengths, and the measured relative optical absorption coefficients were used in Eqs. (1) and (2) to calculate the ratio between blue and red ink in the mixture. The image and the calculated percentile of red ink are presented in Fig. 6. Overall, the calculated percentile map shows good agreements with the real value, which is 50%. However, some fluctuations are also observed on the calculated percentile map. The fluctuations are generally within 10%. The result demonstrates the uncertainty associated with the blood oxygenation measurement result in Fig. 5.

4 Summary

We have applied an optimized curved array photoacoustic system developed previously to small animal brain imaging. In this paper, we reported that nearly real-time imaging with this system is possible. Additionally, ultrasonic gel coupling, instead of water coupling, was used in obtaining the nearly real-time images. Using the new system, we have demon-

strated *in vivo* small animal brain cortex imaging. The blood oxygen saturation level on a small animal brain cortex has also been measured. The time-resolved curve in the relative change of blood oxygen saturation level was presented when the animal physiological status changes between hyperoxia and normoxia. An *in situ*, 3-D, whole-brain image with the new system was also shown and compared with MRI images. The results demonstrated that the curved array system is capable of producing reliable PA images for small animal brain study.

Acknowledgments

We thank Song Hu for helpful discussion on SO_2 calculation. This project was sponsored in part by the National Institutes of Health, Grant Nos. R01 NS46214 (BRP) and R01 EB000712.

References

1. C. G. A. Hoelen, F. F. M. de Mul, R. Pongers, and A. Dekker, "Three-dimensional photoacoustic imaging of blood vessels in tissue," *Opt. Lett.* **23**, 648–650 (1998).
2. R. A. Kruger, D. R. Reinecke, and G. A. Kruger, "Thermoacoustic computed tomography—technical considerations," *Med. Phys.* **26**, 1832–1837 (1999).
3. R. O. Esenaliev, A. A. Karabutov, and A. A. Oraevsky, "Sensitivity of laser opto-acoustic imaging in detection of small deeply embedded tumors," *IEEE J. Sel. Top. Quantum Electron.* **5**, 981–988 (1999).
4. K. P. Köstli, D. Frauchiger, J. J. Niederhauser, G. Paltauf, H. P. Weber, and M. Frenz, "Optoacoustic imaging using a three-dimensional reconstruction algorithm," *IEEE J. Sel. Top. Quantum Electron.* **7**, 918–923 (2001).
5. M. Xu and L.-H. Wang, "Biomedical photoacoustics," *Rev. Sci. Instrum.* **77**(4), 041101 (2006).
6. G. Ku and L. V. Wang, "Deeply penetrating photoacoustic tomography in biological tissues enhanced with an optical contrast agent," *Opt. Lett.* **30**, 507–509 (2005).
7. G. Ku, B. D. Fornage, X. Jin, M. Xu, K. K. Hunt, and L. V. Wang, "Thermoacoustic and photoacoustic tomography of thick biological tissues toward breast imaging," *Technol. Cancer Res. Treat.* **4**, 559–565 (2005).
8. X. Wang, Y. Pang, G. Ku, X. Xie, G. Stoica, and L. V. Wang, "Noninvasive laser-induced photoacoustic tomography for structural and functional imaging of the brain *in vivo*," *Nat. Biotechnol.* **21**, 803–806 (2003).
9. M. Li, J. Oh, X. Xie, G. Ku, W. Wang, C. Li, G. Lungu, G. Stoica, and L. V. Wang, "Simultaneous molecular and hypoxia imaging of brain tumors *in vivo* using spectroscopic photoacoustic tomography," *Proc. IEEE* **96**, 481–489 (2008).
10. H. F. Zhang, K. Maslov, G. Stoica, and L.-H. Wang, "Functional photoacoustic microscopy for high-resolution and noninvasive *in vivo* imaging," *Nat. Biotechnol.* **24**, 848–851 (2006).
11. V. Kozhushko, T. Khokhlova, A. Zharinov, I. Pelivanov, V. Solomatin, and A. Karabutov, "Focused array transducer for two-dimensional optoacoustic tomography," *J. Acoust. Soc. Am.* **116**, 1498–1506 (2004).
12. R. A. Kruger, W. L. Kiser, D. R. Reinecke, and G. A. Kruger, "Thermoacoustic computed tomography using a conventional linear transducer array," *Med. Phys.* **30**, 856–860 (2003).
13. S. Park, S. Mallidi, A. Karpiouk, S. Alyamov, and S. Emelianov, "Photoacoustic imaging using array transducer," *Proc. SPIE* **6437**, 643714 (2007).
14. B. Yin, D. Xing, Y. Wang, Y. Zeng, Y. Tan, and Q. Chen, "Fast photoacoustic imaging system based on 320-element linear transducer array," *Phys. Med. Biol.* **49**, 1339–1346 (2004).
15. R. J. Zemp, R. Bitton, M. L. Li, K. K. Shung, G. Stoica, and L. V. Wang, "Photoacoustic imaging of the microvasculature with a high-frequency ultrasound array transducer," *J. Biomed. Opt.* **12**, 010501 (2007).
16. J. J. Niederhauser, M. Jaeger, R. Lemor, P. Weber, and M. Frenz, "Combined ultrasound and optoacoustic system for real-time high-contrast vascular imaging *in vivo*," *IEEE Trans. Med. Imaging* **24**, 436–440 (2005).
17. A. A. Oraevsky and A. Karabutov, "Ultimate sensitivity of time-resolved opto-acoustic detection," *Proc. SPIE* **3916**, 228–239 (2000).
18. R. A. Kruger, W. L. Kiser, D. R. Reinecke, G. A. Kruer, and K. D. Miller, "Thermoacoustic molecular imaging of small animals," *Mol. Imaging* **2**, 113–122 (2003).
19. J. Gamelin, A. Aguirre, A. Maurudis, F. Huang, D. Castillo, L. V. Wang, and Q. Zhu, "Curved array photoacoustic tomographic system for small animal imaging," *J. Biomed. Opt.* **13**, 024007 (2008).
20. F. Huang, A. Maurudis, J. Gamelin, A. Aguirre, D. Castillo, P. Guo, and Q. Zhu, "A fast photoacoustic imaging system based on a curved ultrasound transducer array," in *2007 IEEE 33rd Annual Northeast Bioengineering Conference*, pp. 47–48 (2007).
21. Laser Institute of America, "American national standard for safe use of lasers," ANSI Z136.1-2000, American National Standard Institute, Inc., New York (2000).
22. B. Chance, E. Borer, A. Evans, G. Holtom, J. Kent, M. Maris, K. McCully, J. Northrop, and M. Shinkwin, "Optical and nuclearmagnetic-resonance studies of hypoxia in human tissue and tumors," *Ann. N.Y. Acad. Sci.* **551**, 1–16 (1988).
23. R. L. Barbour, A. Gebrewold, and B. M. Altura, "Optical spectroscopy and cerebral vascular effects of alcohol in the intact brain: effects on tissue deoxyhemoglobin, blood content, and reduced cytochrome oxidase," *Alcohol Clin. Exp. Res.* **17**, 1319–1324 (1993).
24. H. Liu, D. A. Boas, Y. Zhang, A. G. Yodh, and B. Chance, "Determination of optical properties and blood oxygenation in tissue using continuous NIR light," *Phys. Med. Biol.* **40**, 1983–1993 (1995).
25. Y. Xu, L. V. Wang, G. Ambartsoumian, and P. Kuchment, "Reconstructions in limited-view thermoacoustic tomography," *Med. Phys.* **31**(4), 724–733 (2004).